Available online at www.sciencedirect.com
ScienceDirect
Journal of Solid State Chemistry 180 (2007) 564–570
JOURNAL OF SOLID STATE CHEMISTRY
www.elsevier.com/locate/jssc

Mesoporous aluminosilicate ropes with improved stability from protozeolitic nanoclusters

Junlin Zheng[a,b], Dejin Kong[a], Weimin Yang[a], Zaiku Xie[a], Dong Wu[b], Yuhan Sun[b,*]

[a]*Shanghai Research Institute of Petrochemical Technology, SINOPEC, Shanghai 201208, PR China*
[b]*State Key Laboratory of Coal Conversion, Institute of Coal Chemistry, Chinese Academy of Sciences, Taiyuan 030001, PR China*

Received 8 July 2006; received in revised form 6 November 2006; accepted 13 November 2006
Available online 18 November 2006

Abstract

Mesoporous aluminosilicate ropes with improved hydrothermal stability have been prepared through $S^+X^-I^+$ route via self-assembly of protozeolitic nanoclusters with cetyltrimethylammonium bromides (CTAB) template micelles in HNO_3 solution. SEM observation confirmed that high-yield aluminosilicate ropes could be produced under proper HNO_3 concentration. NO_3^- ions had strong binding strength to the CTA^+ ions and tended to form more elongated surfactant micelles, thus fibrous products were fabricated under the direction of these long rod micelles in shearing flow. At the same time, the NO_3^- ions combining with CTA^+ ions generated more active ($CTA^+NO_3^-$) assembly, which effectively catalysed the polymerization of protozeolitic nanoclusters with large volume into highly ordered mesostructures. Compared with normal MCM-41 silica synthesized through $S^+X^-I^+$ route in acidic media, the hydrothermal stability was improved considerably. These protozeolitic nanoclusters survived strongly acidic media and entered into mesostructured framework, which contributed to the improvement of hydrothermal stability.

Keywords: Mesoporous molecular sieves; Fibre; Zeolitic precursors; Hydrothermal stability

1. Introduction

Mesoporous molecular sieves can be synthesized in either the alkaline media [1,2] or the acidic media [3,4]. In the former route, surfactant cations (S^+) and silicate anions (I^-) are organized by strong S^+I^- electrostatic interaction to get mesoporous materials with highly condensed and compact structures. The acidic route is mediated by counterions of opposite charge to that of the surfactant headgroups (solution species are ($S^+X^-I^+$) where X^- is Cl^-, Br^-, NO_3^- and I^+ is silicate cations, respectively) [3]. In $S^+X^-I^+$ assembly route, the weaker surfactant/silicate interaction permits more delicate competition of the kinetics of silica condensation and surfactant/silicate assembly, and the association of S^+X^- determines the structure and morphology of the mesoporous materials [5]. So the acidic route is versatile in morphology tailoring and much exotic morphology including tubular, spherical, and fibrous morphology have been exploited for the mesoporous molecular sieves through this route [6–11]. Especially, mesoporous molecular sieves with fibrous organization have been intensively investigated to explore their unique structure-associated properties and their potential applications in catalysis, separation, optical devices, and controlled polymerization inside nanochannels. Previous literatures have reported the synthesis of mesoporous silica fibres via $S^+X^-I^+$ route in acidic media [11]. During the assembly process, counterions, acid concentration, shearing flow, and temperature have strong influence on the morphology and structure of the mesoporous materials through $S^+X^-I^+$ route. Unfortunately, the hydrothermal stability of MCM-41-type mesoporous molecular sieves synthesized through $S^+X^-I^+$ route in acidic media is extremely poor for weak surfactant/silicate interaction in the assembly process.

The hydrothermal stability of mesoporous molecular sieves appeared to be improved modestly via many methods such as repeated pH adjustment [12], salt effects [13] and post-synthesis restructure [14]. These methods

*Corresponding author. Fax: +86 21 68462283.
E-mail address: mesozheng@hotmail.com (Y. Sun).

0022-4596/$ - see front matter © 2006 Elsevier Inc. All rights reserved.
doi:10.1016/j.jssc.2006.11.017

were suitable to improve the hydrothermal stability of mesoporous molecular sieves synthesized in alkaline media through S^+I^- route. The most significant improvement in the hydrothermal stability of mesoporous molecular sieves, however, came through the use of protozeolitic nanoclusters as building units to produce aluminosilicate mesostructures [15,16]. Protozeolitic nanoclusters, known as "zeolite seeds", promote zeolite nucleation by adopting AlO_4 and SiO_4 connectivity that resemble the secondary building units of a crystalline zeolite [17]. So far, both S^+I^- route (in alkaline media) and S^0I^0 route (in acidic media) have been developed to synthesize hydrothermally stable mesoporous aluminosilicates from protozeolitic nanoclusters [18–21]. The hydrothermal stability of $S^+X^-I^+$ route derived mesoporous molecular sieves is extremely poor, which severely restricts their practical applications. In our previous work, mesoporous aluminosilicates were synthesized from Beta zeolitic precursors through $S^+X^-I^+$ route in HCl media, in which protozeolitic nanoclusters served as primary building units to fabricate mesostructured frameworks [22,23]. However, the sample from Beta precursors only exhibited a broad (1 0 0) diffraction peak in the XRD pattern, indicating the presence of poorly ordered mesostructure. An additional post-synthesis ammonia procedure must be undergone to further improve their mesostructured regularity and hydrothermal stability. The final products were irregular particles in morphology whatever the concentration of HCl solution. Herein, we present a method to synthesize hydrothermally more stable mesoporous aluminosilicate ropes via self-assembly of protozeolitic nanoclusters with cationic template micelles in HNO_3 solution through $S^+X^-I^+$ route.

2. Experimentals

2.1. Synthesis of materials

A typical preparing procedure is as follows: (1) Zeolite Beta precursor solution containing abundant protozeolitic nanoclusters was prepared according to the previous literature [20]. 0.3 g sodium aluminates, 0.16 g sodium hydroxide, and 4.8 g fumed silica were added into 25 ml Tetraethylammonium hydroxide (TEAOH 20 wt%) solution, and the molar ratio of $Al_2O_3/SiO_2/Na_2O/TEAOH/H_2O$ was 1.0/60/2.5/22/800. The mixture was transferred into a Teflon-lined stainless steel autoclave and hydrothermally reacted at 140 °C for 4 h to yield Beta aluminosilicate precursors. A portion of the zeolitic precursors were placed in an evaporating dish and dehydrated slowly in a 60 °C vacuum oven. (2) Then the precursor solution (25 ml) was dropwise added into 200 ml HNO_3 solution (1.0–2.5 M) with cetyltrimethylammonium bromide (CTAB) in it, and the molar ratio of $CTAB/SiO_2$ was 0.2. After the mixture was treated at 25 °C for 24 h under the stirring rate of 500 rpm, the solid products were recovered by filtration and dried in air. (3) Assembly of protozeolitic nanoclusters into mesostructured framework through $S^+X^-I^+$ route in HCl media obeyed the above-mentioned procedures except that the HNO_3 solution was replaced by 2 M HCl solution [23]. (4) Normal MCM-41 silica was synthesized through $S^+X^-I^+$ route from tetraethyl orthosilicates (TEOS) according to the literature [3]. The product was also filtered, washed with deionized water and dried in air. Finally, the dried precipitates were all calcined in 550 °C for 6 h to remove the organic templates. The hydrothermal stability of resultant mesoporous molecular sieves was evaluated by age in boiling water for 48 h.

2.2. Characterization of materials

The X-ray diffraction (XRD) patterns of the calcined samples were recorded using a Shimadzu XD-3A X-ray powder diffractometer, which employed Ni-filtered Cu$K\alpha$ radiation and were operated at 40 kV and 30 mA. The N_2 adsorption and desorption isotherms at 77 K were measured using a Micromeritics Tristar 3000 apparatus. The mesostructures were analysed from desorption branches of the isotherms by the Barrett–Joyner–Halenda (BJH) model with Halsey equation for multiplayer thickness. Scanning electron microscopy (SEM) images were recorded on a Hitachi 600 instrument with acceleration voltage of 200 kV. ^{27}Al NMR spectra of the dehydrated zeolitic aluminosilicate precursors and the resultant mesostructured aluminosilicates were recorded on a Bruker MSL-400 spectrometer, and the chemical shifts were referenced to $Al(OH)_6^{3+}$.

3. Results and discussion

3.1. Macroscopic morphology

Fig. 1 gives the SEM micrographs of the calcined products synthesized under different HNO_3 concentrations (1 M, 1.5 M, 2 M, 2.5 M). When the concentration of HNO_3 solution is as low as 1 M, the products are mainly irregular particles (Fig. 1a). With the increase of the acid concentration to 1.5 M, the morphologies of the products change obviously: many short ropes (~100 μm) with flocky edges emerge accompanied with much aluminosilicate debris (Fig. 1b). As the concentration is further increased to 2 M, aluminosilicate ropes in the absolute majority are obtained (Fig. 1c). The length is not uniform, but the longer ones tend also to be the thicker ones. Based on systematic SEM observations, it is estimated that the mean diameter and average length of the ropes are 30 μm and 300 μm, respectively. At higher magnification of the aluminosilicate ropes shown in Fig. 1c, we can clearly find that the aluminosilicate ropes consist of micrometer-sized fibres entwined into hierarchical ropes (Fig. 1e). When the acid concentration is as high as 2.5 M, aluminosilicate ropes disappear completely and irregular particles with smaller size, compared with the products shown in Fig. 1a, dominate the final products (Fig. 1d). So 2 M is the optimum HNO_3 concentration to fabricate aluminosilicate

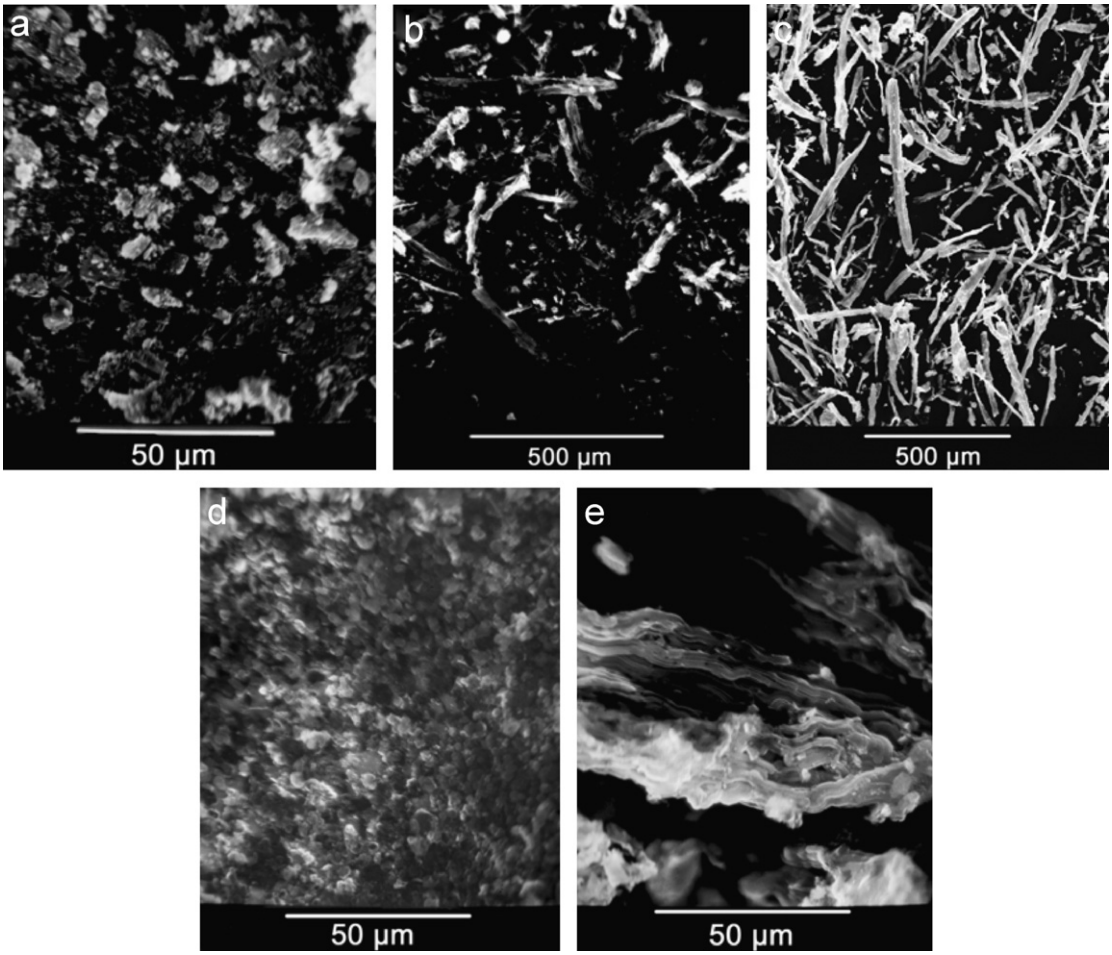

Fig. 1. SEM micrographs of the samples synthesized through $S^+X^-I^+$ route via self-assembly of protozeolitic nanoclusters with CTAB template in HNO_3 solution with different concentrations. (a) 1 M, (b) 1.5 M, (c) 2 M, (d) 2.5 M, (e) 10 times magnification of (c).

ropes from protozeolitic nanoclusters through $S^+X^-I^+$ route, and too high or too low HNO_3 concentrations tend to diminish the morphology tailoring ability.

In $S^+X^-I^+$ route, counterions, acid concentration, and temperature that can influence the "soft" intermediate structure formed under acidic conditions must be considered. When the HNO_3 concentration is 2 M, nitrate ions serving as counterions have stronger binding strength to the surfactant and form more elongated micelles. Shearing flow has the ability to align these elongated micelles from an entangled wormlike structure into a well-aligned one. The aligned micelles are the necessary templates for the formation of aluminosilicate ropes constructed by bundles of aluminosilicate fibres. So mesoporous aluminosilicates with fibrous morphology can be fabricated from protozeolitic nanoclusters conveniently through this particular route. At lower HNO_3 concentration, such as 1.5 M, elongated micelles cannot effectively form in the mixture because of inadequate amounts of nitrate ions, thus irregular particles form accompanying the aluminosilicate ropes under the direction of entangled wormlike micelles. When the acid concentration is 2.5 M, the aluminosilicate ropes disappear completely and irregular particles with smaller size dominate the final products. At $pH < 2$, the polymerization rate of silicate species is proportional to $[H^+]$ [24]. Too high HNO_3 concentration accelerates the aggregation rate of protozeolitic nanoclusters and produces more oligomers of these protozeolitic nanoclusters. More oligomers serve as nuclei seeds of mesostructured framework in the solution and lead to smaller average particle size. So either too high or too low nitric acid concentration does not help the formation of fibrous products.

3.2. Textural properties and improved hydrothermal stability

Fig. 2 shows the XRD patterns of the calcined sample (as shown in Fig. 1c) and normal MCM-41 silica before and after 48 h age in boiling water. Well-ordered material is obtained as evidenced by the XRD patterns of the aluminosilicate ropes (A) before aged in boiling water (a), which has resolved (1 0 0), (1 1 0), and (2 0 0) reflection peaks characteristic of long-range ordered hexagonal symmetry, and the (1 0 0) peak reflects a d_{100} spacing of 4.16 nm. At large angle of 10–40° (see Fig. 3), no obvious

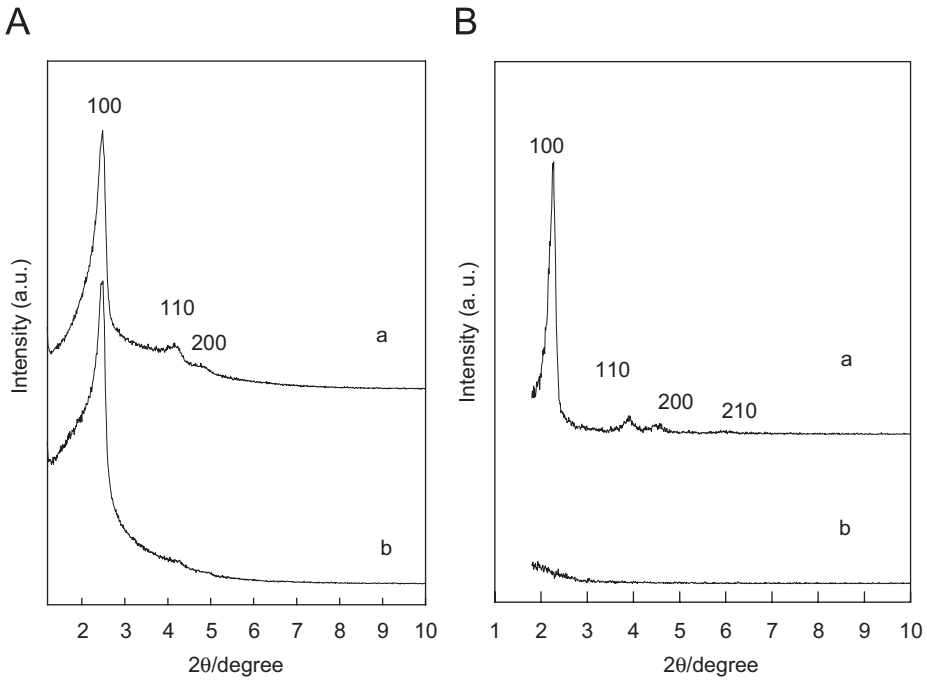

Fig. 2. XRD patterns of the $S^+X^-I^+$ route derived sample via self-assembly of protozeolitic nanoclusters with CTAB template in 2 M HNO_3 solution (A) and normal MCM-41 silica (B) before (a) and after (b) aged in boiling water for 48 h.

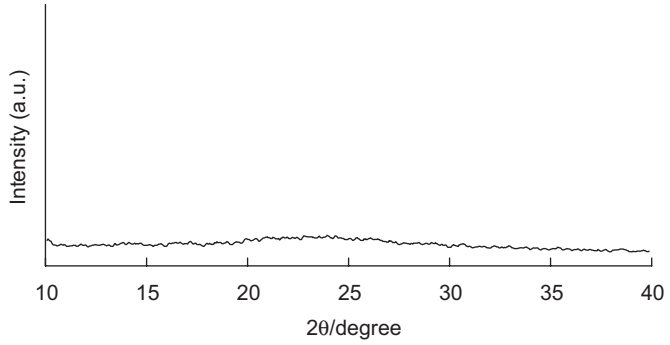

Fig. 3. Large-angle XRD pattern of the $S^+X^-I^+$ route derived sample via self-assembly of protozeolitic nanoclusters with CTAB template in 2 M HNO_3 solution.

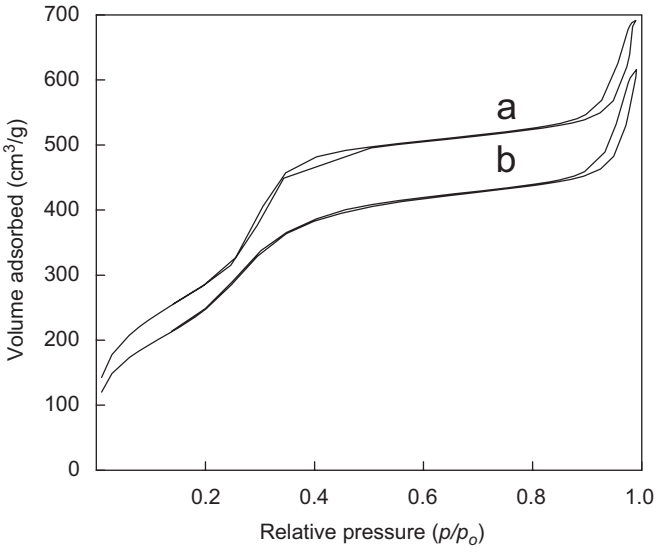

Fig. 4. N_2 sorption isotherms of the $S^+X^-I^+$ route derived sample via self-assembly of protozeolitic nanoclusters with CTAB template in 2 M HNO_3 solution before (a) and after (b) aged in boiling water for 48 h.

diffraction peaks can be observed for the calcined sample, suggesting that no isolated zeolite crystal phase formed in the assembly process of protozeolitic nanoclusters. It was confirmed that acidic media restrained the continuous growth of protozeolitic nanoclusters into zeolite crystals large enough to be detected by XRD in the self-assembly process, so the obtained materials are pure phase mesoporous materials without isolated zeolite crystals [20]. The existence of (1 0 0), (1 1 0), and (2 0 0) diffraction peaks in XRD pattern indicates that hexagonal mestostructures are reserved even after the sample is aged in boiling water for 48 h (b).

Normal MCM-41 silica (Fig. 2B) prepared by using TEOS as silica sources and cationic CTAB surfactants as the templates through $S^+X^-I^+$ route in HNO_3 solution (a) also shows high-quality mesostructure evidenced by the presence of (1 0 0), (1 1 0), and (2 0 0) diffraction peaks, and the d_{100} value is 3.69 nm. But these peaks disappear completely after 48 h age in boiling water (b), which is consistent with the poor hydrothermal stability of normal MCM-41 silica synthesized via $S^+X^-I^+$ route in acidic media.

Fig. 4 is the N_2 adsorption–desorption isotherms of calcined aluminosilicate ropes shown in Fig. 1c. A steep increase occurs in type IV isotherm curve at the relative pressure of $0.30 < p/p_0 < 0.40$, which can be attributed to the presence of highly regular mesostructures (a). The N_2

Table 1
Textural parameters of the resultant sample and normal MCM-41 before and after aged in boiling water

	Age time (h)	d_{100} (nm)	Pore diameter (nm)	Wall thickness (nm)	S_{BET} (m^2/g)	Pore volume (cm^3/g)
Sample	0	3.83	2.50	1.92	1053	0.96
	48	3.66	2.50	1.73	926	0.82
MCM-41	0	3.69	2.50	1.76	1352	0.98
	48	—	—	—	476	0.57

sorption isotherm of mesoporous aluminosilicates after 48 h age in boiling water (b) preserves the sorption behaviour characteristic of regular mesostructures, which is in good agreement with the XRD results.

Calculated from XRD and N_2 sorption results, the textural properties of so-produced materials and normal MCM-41 before and after treatment in boiling water are given in Table 1. The framework wall thickness of so-produced sample and normal MCM-41 silica are 1.92 and 1.76 nm, respectively. The protozeolitic nanoclusters in precursor solution have larger volume and stronger rigidity compared with the nonstructured silicon species hydrolysed from TEOS in the conventional synthesis of MCM-41 silica. So the framework wall thickness increases from 1.76 to 1.92 nm to accommodate the protozeolitic nanoclusters, which contributes to the improved hydrothermal stability partly [25].

The textural properties calculated from XRD patterns and N_2 sorption results reveal the superior hydrothermal stability of the sample to that of normal MCM-41. The BET surface area of the sample decreases slightly from 1053 to 926 m^2/g after 48 h age in boiling water, while the BET surface area of normal MCM-41 decreases sharply by more than 65% after aged. At the same time, the pore volume of the resultant sample decreases from 0.96 to 0.82 cm^3/g slightly, whereas normal MCM-41 loses a large part of its pore volume. XRD and N_2 sorption isotherm results show that the mesostructures of the protozeolitic nanocluster-derived materials are retained, while the mesostructures of normal MCM-41 silica break down completely after 48 h age in boiling water. So the obtained material has remarkably improved hydrothermal stability in contrast to normal MCM-41 silica synthesized in acidic media.

3.3. Integrity of protozeolitic nanoclusters

Fig. 5 gives the ^{27}Al MAS NMR spectra of the dehydrated zeolitic precursors (a) and the sample via self-assembly of protozeolitic nanoclusters with CTAB template in 2 M HNO_3 solution (b). As shown in Fig. 5a, the dehydrated zeolitic precursors have a sole 52.0 ppm chemical shift in the ^{27}Al NMR spectrum. It is showed that the Al species in the precursor solution were entirely tetrahedrally coordinated in the protozeolitic nanoclusters. As to the as-synthesized mesostructured aluminosilicates (Fig. 5b), the chemical shifts at 52.6 and 0 ppm can be assigned to 4- and 6-coordinated Al species, respectively. The overall Al species are mainly 4-coordinated in the final products and the signal of 6-coordinated Al species is rather weak, thus most Al species are incorporated in the mesostructured framework in the form of 4-coordinated Al species (ca 90%) despite the strong acidic media. Contrarily, if the protozeolitic nanoclusters collapsed in the strong acidic media, Al species in the form of Al^{3+} would dissolve and remain in the solution and no tetrahedral Al signal could be found in the ^{27}Al NMR spectra. So the microstructures of protozeolitic nanoclusters have not been destroyed in the strongly acidic media. Pinnavaia [18] and Xiao [20] have also synthesized hydrothermally stable mesoporous aluminosilicates through S^0I^0 pathway from protozeolitic nanoclusters in strongly acidic media where triblock copolymers served as templates. So it is feasible to assemble protozeolitic nanoclusters into mesostructured framework via $S^+X^-I^+$ route in strongly acidic media without degradation of the microstructure of these nanoclusters.

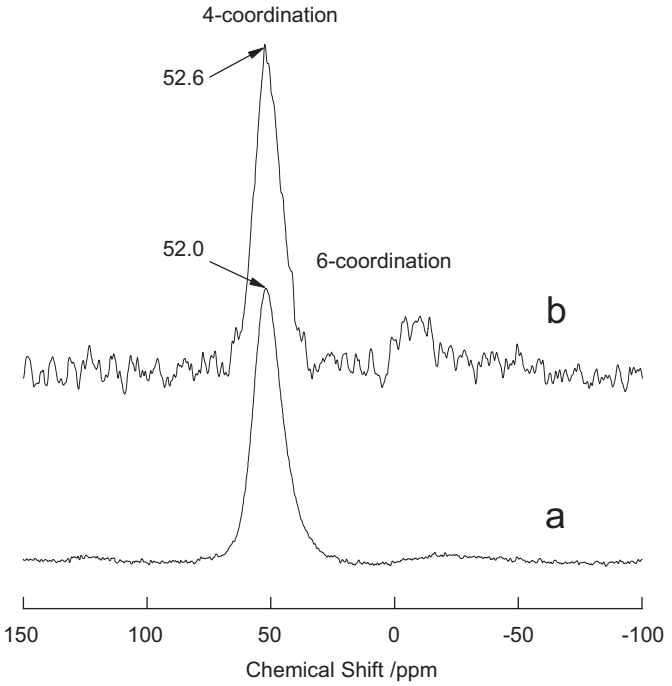

Fig. 5. ^{27}Al MAS NMR of the dehydrated zeolitic precursors (a) and the sample via self-assembly of protozeolitic nanoclusters with CTAB template in 2 M HNO_3 solution (b).

In the present procedure, Al species were incorporated into mesostructured framework, which can be explained that Al species have already entered the framework of protozeolitic nanoclusters in the first step. Alumination process can improve the hydrothermal stability of mesoporous silica [26]. It should be pointed out that the improvement of hydrothermal stability could not merely be attributed to the introduced Al species. Normal mesoporous aluminosilicates synthesized in alkaline route can only survive boiling water age less than 20 h [27]. The hydrothermal stability of current sample is not only superior to normal MCM-41 silica synthesized through $S^+X^-I^+$ route but also higher than normal mesoporous aluminosilicates synthesized through alkaline route. The local structure and connectivity of the silicate units comprising the framework walls are very important factors influencing the hydrothermal stability of mesostructured aluminosilicates [25]. As the protozeolitic nanoclusters were introduced into the framework of the synthesized materials as primary building units, reserved zeolite-like connectivity of tetrahedral SiO_4 and AlO_4 units play a very important role in the improvement of hydrothermal stability [15]. So the introduction and integrity of protozeolitic nanoclusters is the most important contributor to the improvement of hydrothermal stability.

3.4. The effect of counterions

Previous literature [7] have demonstrated that the structural order of the hexagonal mesostructures synthesized from C_{16}TMAB–TEOS–HX–H_2O system under 303 K using different acid source (HX = HCl, HBr, HNO_3, H_2SO_4) followed the order $NO_3^- > Br^- > Cl^- > 1/2SO4^{2-}$. HNO_3 gave the best structural order with the sharpest (1 0 0), (1 1 0), (2 0 0), and (2 1 0) peaks, while HCl got broader (1 0 0), (1 1 0), and (2 0 0) peaks without observable (2 1 0) peak. Protozeolitic nanoclusters are applied as assembly precursors in present procedures, and their assembly behaviour in different acid solution deserves further examination. As discussed in the first two parts, hexagonally ordered mesoporous aluminosilicates with fibrous morphology can be directly fabricated through $S^+X^-I^+$ route via self-assembly of protozeolitic nanoclusters with CTAB template micelles in HNO_3 solution. Fig. 6a is the XRD pattern of mesostructured framework assembled from protozeolitic nanoclusters via $S^+X^-I^+$ route in HCl solution. It should be noted that the diffraction peaks are much less resolved than its counterpart synthesized in HNO_3 media. Highly ordered hexagonal mesostructure can only be obtained after post-synthesis hydrothermal ammonia treatment [23]. It should be noted that no rope-like morphology were seen for the final products whatever the HCl concentrations used. The SEM micrograph (Fig. 6b) shows that the products are all irregular particles. When the protozeolitic nanoclusters were used as assembly precursor, the minor difference of structural orders synthesized in HNO_3 and HCl solution

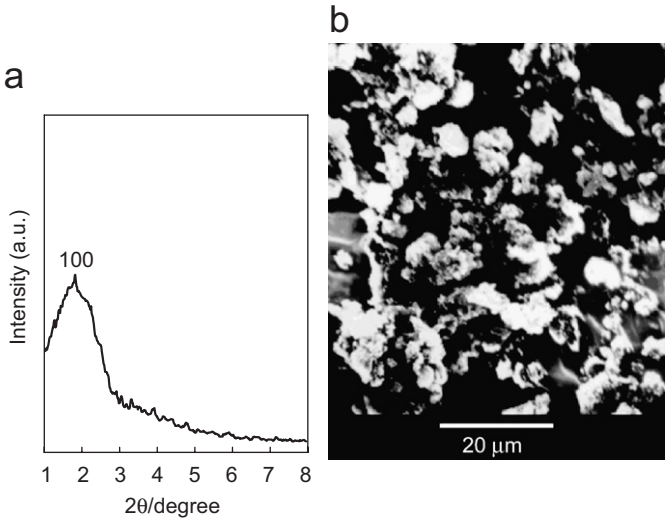

Fig. 6. XRD (a) and SEM micrograph (b) of the $S^+X^-I^+$ route derived sample via self-assembly of protozeolitic nanoclusters with CTAB template in 2 M HCl solution.

were magnified. So the types of counterions have important influence on the assembly behaviour of protozeolitic nanoclusters in $S^+X^-I^+$ route.

The factors involved in determining the formation of mesostructures in acidic route are counterion adsorption equilibrium of X^- on the micellar surface, surface-enhanced concentration of I^+, and proton-catalysed silica condensation near the micellar surface [28]. The S^+I^- surface catalyses the condensation reactions of cationic silica species and condensation step is the rate-controlling step. Thus, the counterions from acid source with the large binding affinity can generate more S^+X^- active sites, which accelerate the silica condensation rate. The counterion with stronger binding strength has more efficiency to catalyse the silica species polymerization. This behaviour should follow the order in the binding affinity of the counterion in the well-known Hofmeister series: $NO_3^- > Br^- > Cl^- > 1/2SO4^{2-}$ [29]. The structure order of the as-synthesized hexagonal phase follows the same order. In HCl solution, the larger volume of the protozeolitic nanoclusters made it relatively difficult to assemble with CTAB templates because of weaker binding strength of Cl^- on surfactant micelles (S^+), which resulted in notable disorder in the product. The nitrate ion gives the strongest counterion association, which neutralizes micellar charge effectively. The stronger charge neutralization would in turn help the formation of more rigid and long micelles and hence better hexagonal structures. So the protozeolitic nanoclusters can be directly assemble into highly ordered hexagonal mesostructures in HNO_3 solution.

4. Conclusions

Mesoporous aluminosilicate ropes with improved hydrothermal stability were prepared via $S^+X^-I^+$ route in HNO_3 media from protozeolitic nanoclusters. NO_3^- ions in

the acidic media improved the long-range order of final products, and fibrous morphology formed under the direction of long rod micelles. The microstructures of protozeolitic nanoclusters survived the strongly acidic HNO_3 media, and the hydrothermal stability of the sample could be improved considerably compared with normal MCM-41 silica through $S^+X^-I^+$ route for the introduction and integrity of protozeolitic nanoclusters. Considering the properties of large surface areas, fibrous morphology, and improved hydrothermal stability, these mesoporous aluminosilicates are potential candidates in catalysis, separation, and optical devices.

Acknowledgments

Financial supports from National Key Basic Research Special Foundation (G2000048001) and the National Nature Science Foundation (29973057) are gratefully acknowledged.

References

[1] C.T. Kresge, M.E. leonowicz, W.J. Roth, J.C. Vartuli, J.S. Beck, Nature 359 (1992) 710.
[2] J.S. Beck, J.C. Vartuli, W.J. Roth, M.E. leonowicz, C.T. Kresge, K.O. Schmitt, C.T.-W. Chu, D.H. Olson, E.W. Sheppard, S.B. McCullen, J.B. Higgins, J.L. Schlenker, J. Am. Chem. Soc. 114 (1992) 10834.
[3] Q.S. Huo, D.I. Margolese, U. Clesia, P.Y. Feng, T.E. Gler, P. Sleger, R. Leon, P.M. Petroff, F. Schüth, G.D. Stucky, Nature 368 (1994) 24.
[4] H. Yang, N. Coombs, G.A. Ozin, Nature 386 (1997) 692.
[5] Q.S. Huo, S.I. Margoleses, U. Ciesla, D.G. Denuth, P.Y. Feng, D.E. Gier, P. Sieger, B.F. Chmelka, F. Schüth, G.D. Stucky, Chem. Mater. 6 (1994) 1176;
D.Y. Zhao, P.D. Yang, Q.S. Huo, B.F. Chmelka, G.D. Stucky, Curr. Opin. Solid State Mater. Sci. 3 (1998) 111.
[6] H.-P. Lin, S.-B. Liu, C.-Y. Mou, C.-Y. Tang, Chem. Commun. (1999) 583.
[7] H.-P. Lin, C.-P. Kao, C.-Y. Mou, S.-B. Liu, J. Phys. Chem. B 104 (2000) 7885.
[8] J.F. Wang, J.P. Zhang, B.Y. Asoo, G.D. Stucky, J. Am. Chem. Soc. 125 (2003) 13966.
[9] M.A. Hatem, Y.S. Lin, Chem. Mater. 15 (2003) 2033.
[10] S.H. Han, W.G. Hou, X. Yan, Z.M. Li, P. Zhang, D.Q. Li, Langmuir 19 (2003) 4269.
[11] H.B. Chan, P.M. Budd, T. deV. Naylor, J. Mater. Chem. (2001) 951.
[12] D. Das, C.M. Tsai, S. Cheng, Chem. Commun. (1999) 473.
[13] J.M. Kim, S. Jun, R. Ryoo, J. Phys. Chem. B 103 (1999) 6200.
[14] R. Mokaya, J. Phys. Chem. B 103 (1999) 10204.
[15] Y. Liu, T.J. Pinnavaia, J. Mater. Chem. 12 (2002) 3179.
[16] J.L. Zheng, Y. Zhang, Z.H. Li, W. Wei, D. Wu, Y.H. Sun, Chem. Phys. Lett. 376 (2003) 136.
[17] R. Ryoo, S. Jun, J.M. Kim, M.J. Jim, Chem. Commun. (1997) 2225.
[18] Y. Liu, T.J. Pinnavaia, Chem. Mater. 14 (2002) 3.
[19] Y. Liu, W.Z. Zhang, T.J. Pinnavaia, Angew. Chem. Int. Ed. 40 (2001) 1255.
[20] Y. Han, F.-S. Xiao, S. Wu, Y.Y. Ying, X.J. Meng, D.S. Li, S. Li, J. Phys. Chem. B 105 (2001) 7963.
[21] Z.T. Zhang, Y. Han, F.-S. Xiao, S.L. Qiu, L. Zhu, R.W. Wang, Y. Yu, Z. Zhang, B.S. Zou, Y.Q. Wang, H.P. Sun, D.Y. Zhao, Y. Wei, J. Am. Chem. Soc. 123 (2001) 5014.
[22] J.L. Zheng, Y. Zhang, D. Wu, Y.H. Sun, Acta Phys.-Chim. Sin. 19 (2003) 907.
[23] J.L. Zheng, S.R. Zhai, D. Wu, Y.H. Sun, J. Solid State Chem. 178 (2005) 1630.
[24] R.K. Iler, The Chemistry of Silica, Wiley, New York, 1979.
[25] T.R. Pauly, V. Petkov, Y. Liu, S.J.L. Billinge, T.J. Pinnavaia, J. Am. Chem. Soc. 124 (2002) 97.
[26] R. Mokaya, Chem. Phys. Chem. 3 (2002) 360.
[27] A. Corma, Chem. Rev. 97 (1997) 2373.
[28] Q.S. Huo, S.I. Margoleses, U. Ciesla, D.G. Denuth, P.Y. Feng, D.E. Gier, P. Sieger, B.F. Chmelka, F. Schuth, G.D. Stucky, Chem. Mater. 6 (1994) 1176.
[29] D.N. Rubingh, P.M. Holland, in: Surfactant Science Series 37, Marcel Dekker, New York, 1991.